POLITECNICO DI TORINO
Repository ISTITUZIONALE

Vibration parameters identification of turbomachinery rotor blades under transient condition using Blade Tip-Timing measurements

(Article begins on next page)

16 May 2024

Vibration parameters identification of turbomachinery rotor blades under transient condition using Blade Tip-Timing measurements

S. Bornassi*, T.M. Berruti, C.M. Firrone, G. Battiato

Dipartimento di Ingegneria Meccanica e Aerospaziale, Politecnico di Torino, Corso Duca degli Abruzzi, 24, 10129 Torino, Italy

Abstract

During run ups and run downs, the rotating blades are subjected to fluctuating forces with time dependent frequencies and the dynamic response of the blades around the resonance crossings deviates from the stationary response. This paper presents a procedure to identify the vibration parameters of rotating blades under this non-stationary condition. An analytically based solution of a single degree of freedom (SDOF) system exposed to a transient harmonic excitation with linear time varying frequency is used for parameters identification. This analytical model is fitted into the Blade Tip-Timing (BTT) data and the vibration parameters are determined by a least square optimization technique. A numerical simulator based on a lumped parameter model of the bladed disk assembly is employed to demonstrate the method performance. Afterwards, the accuracy of the method is proved by testing it on the experimental data acquired by BTT and strain gauges on a rotating bladed disk.

Keywords: Transient resonance passage, Linear sweep rate, Vibration parameters identification, Tip-timing method, Strain gauge

---

*Corresponding author.
Email address: `saeid.bornassi@polito.it` (S. Bornassi)

1. Introduction

With the growing trend, worldwide, of using renewable energy resources in power generation, the power plants are more and more required to feed the power grid on demand. This means increasing operational flexibility of the power plants [1, 2]. In such circumstances, the turbines (gas or steam) need to start-up, shut-down and changing the loads, always more frequently and more rapidly. Therefore, the turbine blades can cross the resonances very quickly leading to a non-stationary (or transient) characteristic in the vibratory response. This causes a response of the blades different from the Frequency Response Function (FRF) that normally occurs in the stationary (or steady state) condition, when the sweep rate is very slow.

There is a critical value of the sweep rate above which the transient effect becomes significant [3] and this effect is more relevant in the lightly damped systems. Aero-engines often operate at an acceleration rate above the critical value [4] and in such circumstance the blade response in resonance tends to show the beatings. Fig. 1 shows the typical vibration response curves for both steady state and transient resonance conditions. As depicted in this figure, non-stationary effect would lead to some major consequences in the vibration response:

— the presence of the beating phenomenon after the maximum amplitude.

— the decreasing of the maximum amplitude.

— the shifting of the maximum peak to a higher frequency.

Several authors have studied the response of a simple vibration system subjected to the swept-frequency excitations. For the first time, Lewis [5] in 1932 analyzed the dynamics of a damped SDOF system when the frequency of the applied force varies linearly with time, he gave an expression for the envelope function that contained the peak of the response. Fearn and Millsaps [6] derived simple algebraic expressions for the maximum amplitude and the frequency in which the maximum amplitude occurs. They obtained results for an undamped SDOF system subjected to a linear frequency sweep excitation. Using a different approach, Markert and Seidler [7] proposed an exact analytical solution for the harmonic forced response of a SDOF system crossing resonance in run-up or run-down with constant acceleration. They presented three approximate formulas for the response envelope and the estimations of the maximum amplitude and its corresponding frequency. Recently, Reed and Kabe [8] extended and completed previously published works by presenting closed form
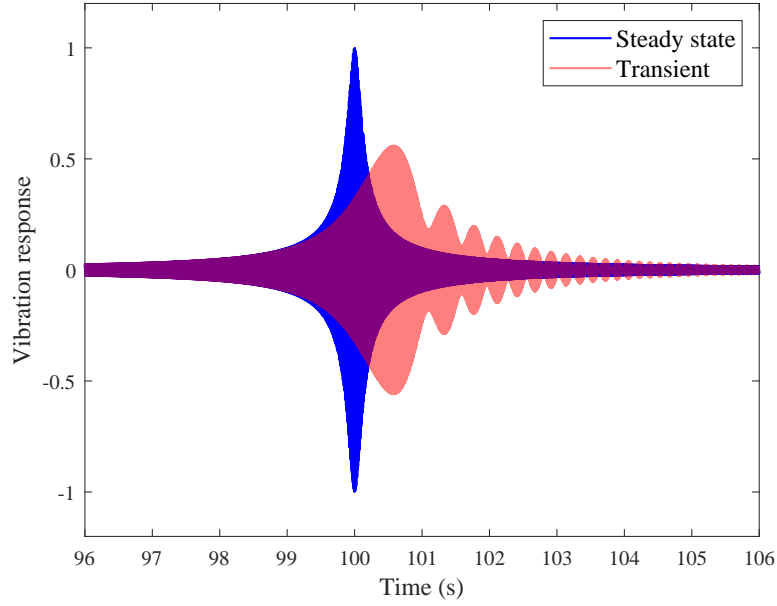
Figure 1: Vibration responses in stationary and transient resonance sweeps.

solutions for both linear and octave swept-frequency excitation of an SDOF system. They compared the results with those obtained by the direct numerical integration of the equations of motion.

Turbine blades are critical components that can be subjected to High Cycle Fatigue (HCF) failure caused by high amplitude vibrations. High amplitudes are excited when critical speeds are reached by the disk in acceleration and deceleration phase. The researchers made significant efforts on the investigation of the bladed disks forced response [9, 10]. Most of the papers were focused on the stationary operating conditions, while relatively few works in literature deal with the transient vibration response. Ayers *et al.* [4] developed a method based on a fundamental mistuning model to predict the vibratory response of a bladed disk under high acceleration rates of the engine. They showed a critical acceleration rate above which the transient effects has an influence on the blade response. Hartung [11] described a new numerical approach to compute the passage through the resonance of a turbine blade. The experimental results were compared with those obtained by a simplified multi body model with a very good agreement. Bonhage *et al.* [12] investigated the transient nonlinear vibration response of the turbine blades by considering the friction damping. This study actually provided a simple guideline on how to design shrouds to minimize amplitudes during resonance crossings. In a later work [13, 14] they studied the amplitude amplification of the mistuned blades in transient resonance crossings. Using a lumped mass model, they

showed that the maximum amplitude of the transient vibration response can exceed the maximum amplitude of the steady state response up to 20%, and for the first time the occurrence of this phenomenon was proven in experiment. The transient vibration analysis of a mistuned bladed disk crossing the resonance was carried out by Kaneko [15], by using both the conventional modal analysis method and the numerical integration method. For the worst mistuning pattern, the effects of the acceleration rate and the blade damping on the transient vibration response were examined in detail and it was concluded that by increasing the acceleration rate, the effect of mistuning becomes smaller. Lubbe and Siewert [16] evaluated the effect of a small variation of the tuned blades resonance frequency and of the intentional mistuning on the resonance amplitudes under transient inertia forces induced by the rotor imbalance.

The measurement of the rotating blades vibration amplitude with high accuracy is of great interest during the health monitoring of the turbomachinery, as well as in the rotating experimental setups designed for dynamic models validation. The experimenters should consider that, using the traditional identification methods [3] to extract the vibration parameters from a dynamic response curve obtained in transient condition, leads to overestimate the maximum amplitude, the damping and the associated natural frequency. Carassale *et al.* [17] proposed a procedure for modal parameters identification, in particular the damping, of turbine blades during a non-stationary working conditions, they validated it by a numerical simulations. They used the concept of Wavelet Transform to compute the amplitude of the signal, afterwards they applied an FRF fitting on the signal, based on a single DOF system, in order to determine the damping value. The effect of the natural frequency variation over time was also considered in their FRF fitting. In [18] they expanded their method to the case of dynamically-coupled bladed disks with mistuned blades. They actually presented a multi DOF identification technique. More details on the Wavelet based procedure and validation of the method can be found in Carassale *et al.* [19]. Their work was also supported by measurements obtained by strain gauges in a spin experimental setup.

Strain gauges are traditionally employed in rotating blade vibration measurement. They have the advantage of high accuracy and well-established signal processing algorithms. However the strain gauges have limited lifetime, their data transmission is very complex in rotating systems, they are intrusive and they monitor only the blades on which they are glued. A measurement technique alternative to strain gauges has gained considerable attention during last decades in the turbomachinery community. This technique is the Blade Tip Timing (BTT) which is non-contact and has the main advantage to simultaneous monitor

all the blades. The BTT technique works based on the concept of time of arrival of the blades passing in front of stationary sensors. The major shortcoming of this method is the undersampling of the sensors signals, which complicates the post-processing of the signals and can lead to inaccurate results.

Different methods have been developed in literature to post-process of the BTT sensors signals. These methods mainly includes single parameter method [20], two parameters plot method [21], Sine fitting method [22], determinant method [23], autoregressive method [23], and sensor waveform analysis method [24]. Based on these methods, further applications, developments and modifications were also proposed. An improvement of the single parameter method was proposed by Heath and Imregun [25] in order to consider the effects of blade vibration on the time of arrivals. Schlagwein and Schaber [26] presented a multi-degrees-of-freedom evaluation method to obtain the vibration parameters in the mistuned systems. The method was tested on both simulated and measured data. In his PhD thesis, Russhard [27] developed methods to optimize the position of sensors in presence of single and multimode synchronous vibration, single mode asynchronous vibration and to identify the nodal diameters. Guo *et al.* [28] developed a novel technique to identify vibration parameters without the need of the once-per revolution sensor. They validated the method experimentally; their results were consistent with the results obtained by the traditional single-parameter method. Rigosi *et al.* [29] made a revision of the two-parameters plot method in order to determine the Engine Order (EO). The method was tested on measurements of BTT optical probes on a rotating bladed disk. Battiato *et al.* [30] assessed the capabilities and performance of a latest generation BTT system to study the synchronous vibration on different bladed disks. They also proposed an original method for nodal diameter identification in the systems with small mistuning. A successful application of a BTT measurement system on a heavy-duty gas turbine for design validation purposes was presented by Bornassi *et al.* [31]. The resonance parameters of the blades were detected through the application of the classical Sine fit method. Bornassi *et al.* [32] recently introduced a fitting procedure based on the steady state harmonic response of a 2DOF system in order to identify the vibration parameters when the resonance peak is split in two peaks.

Most of the papers on identification of vibration parameters from BTT measurements consider that the rotating system vibrates in stationary conditions. When the system is not in stationary conditions, because the rotation speed is changing very fast, using identification methods for stationary systems leads, also in this case, to wrong results in both resonance frequency and damping identification. This paper is focused on those cases when the BTT

measurements, but also strain gauge measurements, are carried out during crossing of a resonance in non-stationary operation. In particular the paper proposes a transient model to fit the data based on the SDOF resonator model developed by Markert and Seidle [7] for the case of transient passage across a resonance. In the first part of the paper, the transient model capabilities are proved using a numerical simulator consisting of a lumped mass model of a bladed disk. Then, the use of the transient model is validated on experimental results. The test campaign includes the acquisition, at the same time and on the same rotating disk, of BTT signals and strain gauge signals. By fitting the proposed transient model on the BTT sensors data or strain gauge data, the main vibration parameters (natural frequency and damping) can be obtained. Five fiber optical BTT sensors located at different angular positions are used to measure the blade tip vibration. Two blades are also equipped with strain gauges in order to provide a reference for BTT validation. Data fitting is performed via a nonlinear least square optimization technique. The vibration parameters extracted by both BTT sensors data and strain gauges data are compared to validate the proposed transient model.

The paper is structured as follows. Section 2 describes the principle of the BTT technique, the mathematical background of the proposed fitting transient model, the implementation of the model on the BTT measurement and the fitting procedure. Section 3 presents the validation of the model capability on a numerical test case. Section 4 presents the model validation by treating experimental data from BTT and strain gauge.

2. Theoretical basis and methodology

2.1. Fundamentals of the BTT technique

In Figure 2 a schematic representation of a BTT measurement system is depicted. A BTT set-up consists of a number of non-contact sensors mounted on a turbomachinery casing. The sensors are arranged circumferentially around the rotor blades with the sensors faces pointing in radial direction towards the blade tip. The sensors position [33] is chosen according to the number of resonances of interest to be captured over a given speed range. It is in fact a good practice, before performing a tip timing measurement, to have an idea in advance about the ranges of possible rotational speeds where the resonances can happen. This can be obtained by computing the Campbell diagram, through a finite element model of the bladed disc, identifying the speed regions where the EO lines cross the natural frequency lines.

The principle of the BTT method is based on the measurement of the time of arrival, that is the time elapsed for a blade to travel between the sensors. The time of arrival of a vibrating blade is different from that of a non-vibrating blade. The time that a non-vibrating blade takes to travel a certain angular distance θ is expressed as

$$t_e = \frac{\theta}{\Omega} \tag{1}$$

in which Ω, the rotating speed of the shaft, is a known parameter and it is obtained by the Once-Per-Revolution (OPR) sensor.

A vibrating blade will arrive at the sensor slightly sooner or later than a non-vibrating blade. Therefore, the actual time of arrival measured for a vibrating blade has a slight lead or lag Δt, given by

$$t_a = t_e \pm \Delta t \tag{2}$$

By determining the tiny difference between the expected and measured times of arrival, the blade tip deflection d can be calculated as

$$d = R\,\Omega\,\Delta t \tag{3}$$

where R is the radius at the measurement point of the blade.

The rotational speed of the bladed disk can increase or decrease with low or high speed rate. The level of this speed rate will modify the shape of the signals acquired by the sensors. To give a clearer picture, a typical blade vibration response and the corresponding BTT signals detected by the sensors (d) are plotted in Fig. 3 for both the stationary and non-stationary resonance crossings. By the post-processing of the BTT sensor signals shown by the red and blue curves in Fig. 3, the vibration parameters of the blade can be obtained. If the peak is very well isolated from the other resonance peaks, the data can be treated as coming from a single degree of freedom (SDOF) vibrating system [32].

The next paragraph presents the solution of the equation of motion of a SDOF system vibrating in transient condition, that is with excitation frequency increasing (or decreasing) with time.

2.2. Transient SDOF model

The equation of motion of a viscously damped SDOF vibrating system, subjected to an external force $f(t)$, is:
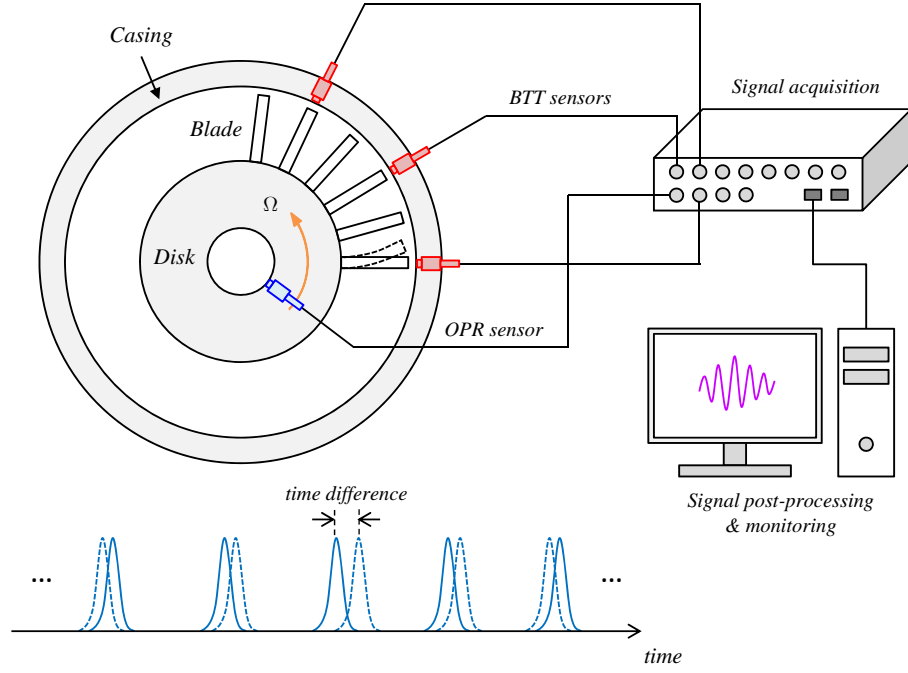
$$m\ddot{x} + c\dot{x} + kx = f(t) \tag{4}$$

7

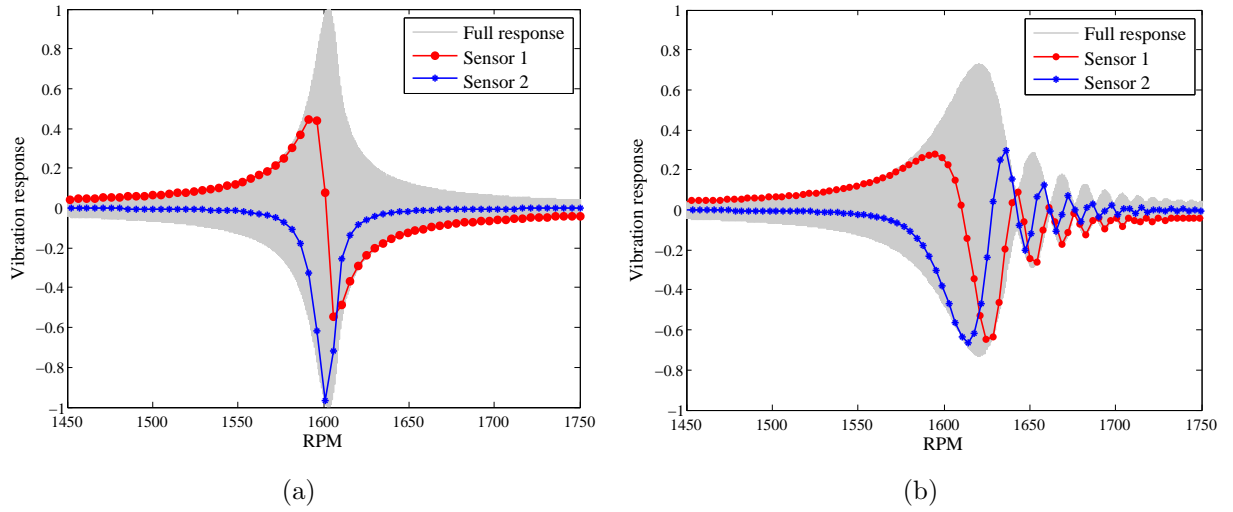Figure 2: Schematic illustration of a BTT measurement system.

(a)

(b)

Figure 3: Vibration response and the associated BTT sensors data in the resonance passages, (a) Stationary (0.1 Hz/s), (b) Transient (1.67 Hz/s).

8

where m, c and k are the mass, damping and stiffness of the system, respectively.

The steady-state solution of this system under a stationary harmonic excitation $f(t) = f_0 \cos(\omega t)$, where ω is constant, is expressed as

$$x = |Q| \cos(\omega t - \psi) \tag{5}$$

where

$$Q = |Q| e^{-i\psi} \; ; \quad |Q| = \frac{\delta_{st}}{\sqrt{(1-r^2)^2 + (2\zeta r)^2}} \; ; \quad \tan(\psi) = \frac{2\zeta r}{1-r^2} \; ; \quad r = \frac{\omega}{\omega_n} \; ; \quad \delta_{st} = \frac{f_0}{k} \tag{6}$$

where ζ is the damping ratio and δ_{st} is the static deflection parameter.

It must be emphasized that this solution is valid only when the excitation frequency ω is constant or almost constant since ω is variable with a very low (infinitesimal) sweep rate. On the contrary, for finite and high sweep rates, the transient effect must be taken into account.

For a general external force, the particular solution of Eq. 4 after neglecting the homogenous response (dissipated due to damping) can be written as a convolution integral [34]:

$$x(t) = \int_0^t f(s) h(t-s) \, ds \tag{7}$$

where

$$h(t) = \frac{1}{\omega_d} e^{-\zeta \omega_n t} \sin(\omega_d t) \; ; \quad \omega_d = \omega_n \sqrt{1 - \zeta^2} \tag{8}$$

In the case of a transient harmonic excitation force, with a frequency not constant but variable with an arbitrary sweep rate, it does not exist any closed form solution for the integral in Eq. 7. In the particular case of a linear sweep rate of the excitation frequency, Markert and Seidle [7] introduced an approximate formula as solution of the integral of Eq. 7. This approximate solution is a non-stationary response which has a form similar to the stationary response in Eq. 5:

$$x(\tau) = |Q(\tau)| \cos(\varphi(\tau) - \psi(\tau)) \tag{9}$$

where $\tau = \omega_n t$ is the non-dimensional time variable.

For an EO excitation and a linear rotating speed sweep $\Omega(t) = at + \Omega_0$, the term $\varphi(t)$ is obtained as

$$\varphi(t) = EO \int_0^t \Omega(t) \, dt = EO \left(\frac{a}{2} t^2 + \Omega_0 t + \beta_0 \right) \tag{10}$$

9

where a and Ω_0 are the sweep rate of the rotating speed and the starting rotating speed (at $t = 0$) respectively and β_0 is the initial phase angle.

By using the non-dimensional time variable, Eq.10 can be rewritten in the form

$$\varphi\left(\tau\right) = \frac{\alpha}{2}\tau^2 + \eta_0\tau + \beta \tag{11}$$

where

$$\alpha = \frac{EO\,a}{\omega_n^2} \;\; ; \;\; \eta_0 = \frac{EO\,\Omega_0}{\omega_n} \;\; ; \;\; \beta = EO\beta_0 \tag{12}$$

where α indicates the non-dimensional sweep rate of the excitation frequency and η_0 is the non-dimensional starting frequency.

Markert and Seidle [7] proposed the approximation for the complex amplitude function $Q\left(\tau\right)$ as:

$$Q\left(\tau\right) = B\left\{2e^{-v^2} + \frac{i}{\sqrt{\pi}}\frac{2v}{2v^2 - 1}\right\} \tag{13}$$

in which

$$B = \frac{1 - i}{4\sqrt{1 - \zeta^2}}\sqrt{\frac{\pi}{\alpha}}\,\delta_{st} \;\; ; \;\; v = -\frac{1 + i}{2\sqrt{\alpha}}\left(\alpha\tau + \eta_0 + i\lambda\right) \;\; ; \;\; \lambda = -\zeta + i\sqrt{1 - \zeta^2} \tag{14}$$

This approximation only holds for the regions of $r > \sqrt{1 - \zeta^2} + \zeta$ and $r < \sqrt{1 - \zeta^2} - \zeta$ in the positive ($\alpha > 0$) and negative ($\alpha < 0$) sweep rates, respectively. These regions correspond to after and before the stationary resonance frequency.

For comparison, the approximate result and the exact solution are shown in Fig. 4 for a positive sweep rate. It can be seen that the approximate formula successfully follows the exact solution in a limited portion of the response. In detail the approximate formula is able to capture the transient effect and the associated beating phenomenon in the portion of the response after the maximum amplitude.

2.3. BTT representation of the transient SDOF model

Eq. 9 should be discretized over time in order to represent the response of the blade seen by the sensors in the stationary frame. In fact, the sensors see the blades once at each revolution. The angular distance traveled by a blade to pass in front of a sensor located in an installation angle of θ at the kth revolution can be calculated with the following relation:

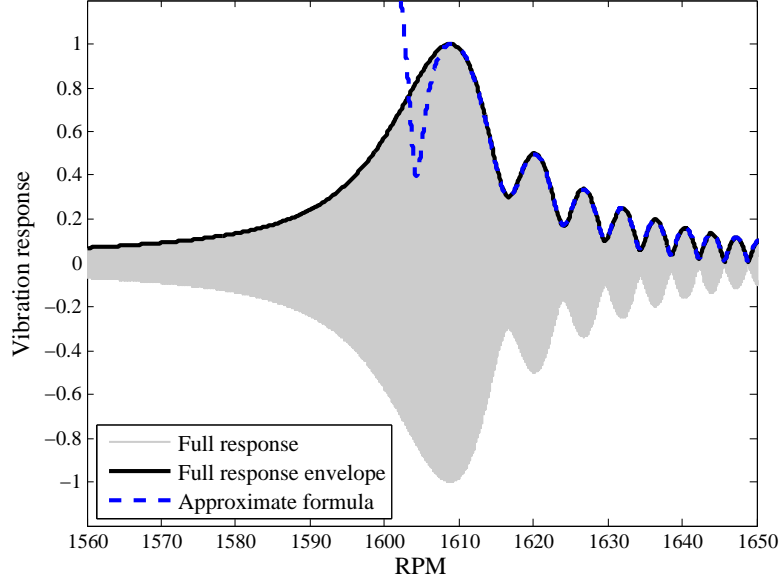$$\varphi\left(\tau_k\right) = EO\left(\varepsilon + \theta + 2\pi k\right) \tag{15}$$

Figure 4: Comparison of the approximate solution with the exact response.

where ε denotes the angular position of the blade at $t = 0$.

By substituting Eq. 15 into Eq. 9 and dropping the term $2\pi k$, the response of the blade captured by each sensor in the kth revolution can be obtained as

$$x_k = |Q\left(\tau_k\right)| \cos\left(EO\theta + \bar{\varepsilon} - \psi\left(\tau_k\right)\right) \tag{16}$$

in which $\bar{\varepsilon} = EO\varepsilon$.

For the sake of simplicity, the blade steady state deflection (static offset) is neglected in Eq. 16. This relation can be used to mimic the signals measured by the sensors during the transient passage through the resonance as shown by the blue and red curves of Fig. 3. Hence starting from the real tip timing sensors signals, this formula can be used for identifying the vibration parameters via a reverse calculation. This can be accomplished by means of a curve fitting procedure.

It should be noted that Eq. 16 is not only a function of the rotating speed, the EO, the sensor installation angle and the phase angle, but it is also a function of parameters related to the blade dynamics (natural frequency, damping ratio and the static deflection parameter). Rotating speed and sensor positions are already known while the rest of the parameters are unknowns. By specifying the EO, the unknown parameters can be identified by fitting Eq. 16 to the BTT data recorded by the sensors over the resonance region. The

11

procedure of the method implementation is shown in Fig. 5.

Here an important point should be stressed. As mentioned in the previous subsection, the approximate transient response formula of Eq. 16 agrees with the exact solution after/before (acceleration/deceleration) the point associated with the stationary resonance frequency towards the beating phenomenon. This means that only the data of the sensors that fall within this region must be retained in the fitting by the transient response model. On the contrary in the case of fitting by a traditional steady state response model, the data recorded over the entire resonance region are included in the fitting procedure. From a practical point of view, a steady state pre-fitting could help to identify the region of the curve to include in the transient fitting. The point corresponding to the peak amplitude of the steady state fitted curve can in fact be used as a reference. Only the data of the sensor that falls between the reference point and the end of the beating are fitted by the transient response model.

A Nonlinear least square optimization technique is used for the data fitting. The quality of the fitting is evaluated by the magnitude of the residual. The computational cost of the fitting can be substantially reduced by assigning constraints to the unknown parameters. This also results in more accurate predictions. From a practical point of view, prior information from FEM calculation (Campbell diagram) or previous results from modal tests can be useful for setting the initial guesses of the unknown parameters. Typically, the starting point for the natural frequency is set equal to the possible EO multiplied by the approximate rotating speed at the resonance. The initial guess of the damping value is selected in a typical range from 0.0001 to 0.01. In order to avoid local minimum, it is useful to force the optimizer to start from multiple starting points.

If the EO is known in advance, one sensor is enough to estimate the unknown parameters. On the contrary, if the EO is unknown, more than one sensor (at least two sensors for the case with zero static offset and three sensors for the case with nonzero static offset) are needed. The best estimations of the parameters can be achieved by repeating the fitting analysis for different possible EO values. The residual value of the fitting procedure will be minimum for the correct EO value. Having a numerical Campbell diagram, already available before the BTT measurements could be a useful help for selecting the most likely EO values to be fed in the fitting procedure.

The fitting model here presented is valid for the case of a blade response showing one peak at the resonance frequency. For cases where the resonance peak is split into two peaks, due to the presence of mistuning, it would be necessary to extend this model to a two DOFs model.
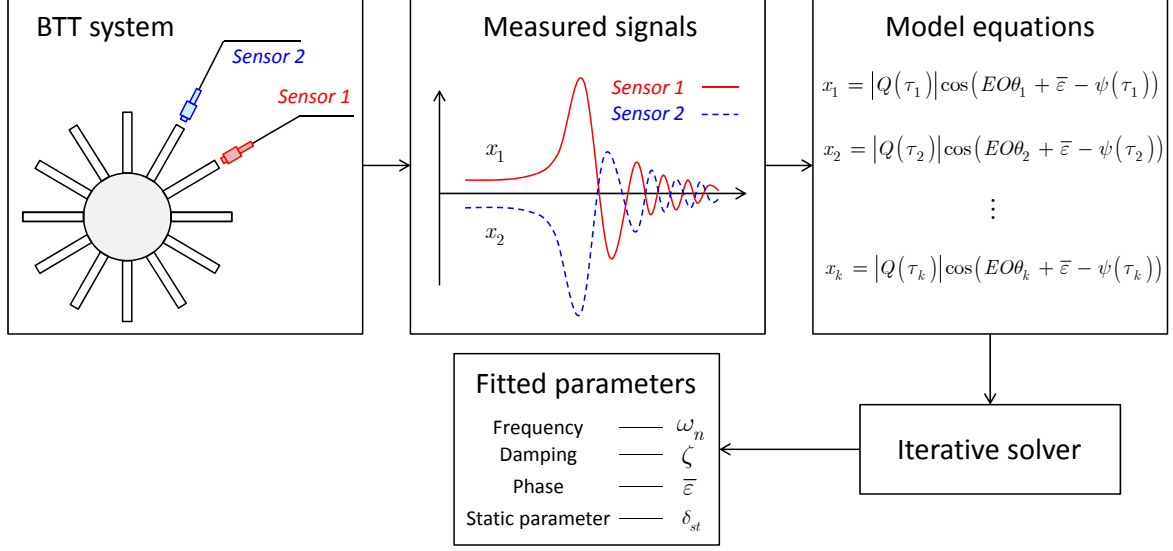
Figure 5: The presented method implementation procedure.

3. Numerical validation

3.1. Numerical test case

A numerical test case with known parameters was created in order to simulate the experiment and to produce data on which to verify the accuracy and robustness of the proposed transient fitting model. The test case is a lumped parameter model of a bladed-disk assembly as shown in Fig. 6. Using this test case the proposed transient fitting model can be tested on different simulated signals coming from different resonance conditions.

As depicted in Fig. 6, each single bladed-disk sector is modeled by a set of masses and springs. Two degrees of freedom are considered for each sector, one representing the blade motion and the other one representing the disk motion: the mass and stiffness of the blades are represented by m_b and k_b, while m_d and k_d are the mass and stiffness of the disk. The connections between adjacent sectors are provided by the coupling springs, named k_c. The chosen parameter values for the bladed disk model are listed in Table. 1.

The mathematical equations of motion of the bladed disk lumped parameter model with viscous damping can be expressed as

$$\mathbf{M}\ddot{\mathbf{q}}(t) + \mathbf{C}\dot{\mathbf{q}}(t) + \mathbf{K}\mathbf{q}(t) = \mathbf{F}(t) \tag{17}$$

where $\mathbf{M}$, $\mathbf{C}$ and $\mathbf{K}$ are the mass, damping and stiffness matrices of the system. Details of these matrices could be found in Refs. [35, 36]. $\mathbf{F}$ is the excitation force vector and $\mathbf{q}$ is the
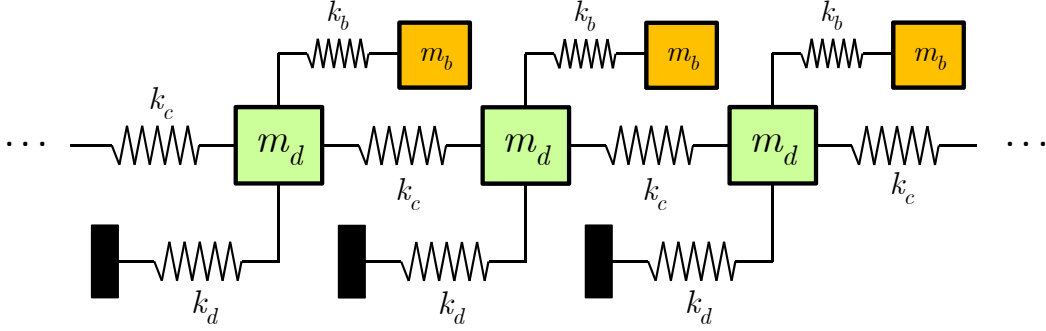
13

Figure 6: Lumped mass model of the bladed disk assembly used for simulation.

vector of the vibration response. The damping is assumed to be a proportional damping expressed as a linear combination of the mass and stiffness matrices as follows:

$$\mathbf{C} = \alpha \mathbf{M} + \beta \mathbf{K} \tag{18}$$

where α and β are real positive known constants.

The curve of natural frequencies versus the nodal diameters for the first family of modes is shown in Fig. 7.

In order to mimic the excitation force in a rotating bladed disk, the force is assumed to be a traveling wave excitation applied on each blade. This means that on the ith blade, the excitation force is:

$$F_i(t) = F_0 \cos\left(\omega t - \frac{2\pi EO}{N}(i-1)\right) \quad ; \quad i = 1, 2, 3, \dots, N \tag{19}$$

in which F_0 is the amplitude of the exciting force, N is the number of blades and ω is the excitation frequency represented by

$$\omega = EO\,\Omega \tag{20}$$

The vibration response of the blade is obtained by numerically solving (by Runge-Kutta method) the ordinary differential equations of motion of the system given in Eq. 17. The BTT sensors signals are then generated by sampling the computed data of the response at discrete values of time corresponding to the times of arrival under each sensor. Two sensors virtually placed at the installation angles of 0 and $pi/4$ collects the BTT samples.

The fitting by the transient model explained in the previous section is then applied to the simulated sensor data, to detect the vibration parameters.

14

Table 1: Parameters of the lumped bladed disk model.

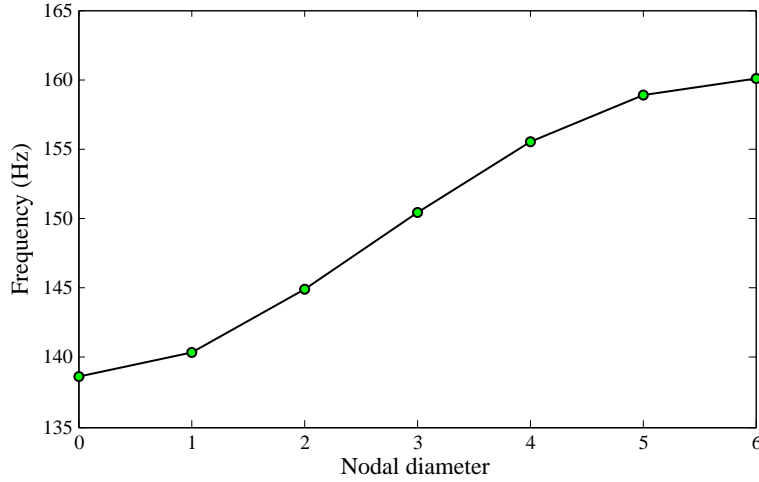| Parameter	Symbol	Value	Unit
Number of blades	N	12	
Blade mass	m_b	1	kg
Disk sector mass	m_d	4	kg
Blade stiffness	k_b	1.80e6	N/m
Disk stiffness	k_d	4.35e6	N/m
Coupling stiffness	k_c	5.00e5	N/m

Figure 7: Natural frequencies of the lumped model vs. nodal diameters for the first mode family.

3.2. Numerical results

Several test conditions can be simulated through the numerical model. The numerical model of the bladed disk allows to set a priori vibration parameters that will afterwards be determined by the fitting of the sensors data. The BTT sensors signals are then generated by sampling the computed numerical response at discrete points corresponding to the position of the sensors. The generated sensor signals are then fitted by both the transient model and the classical steady state fitting model. The vibration parameters values obtained by the fitting are compared with their true values set, since the beginning, in the numerical model of the bladed disk. The response curves obtained by the two fitting models are also compared with the exact solution numerically computed. This validation is performed for different conditions of EO, acceleration rate, and also by introducing noise in the simulated sensor signals. These different cases are presented in the next subsections.

3.2.1. Different resonance cases

The two first cases under study are the two resonances at ND 6 and ND 5 respectively excited by the EO of 6 and 7. For these simulations, the sweep rate of the rotating speed is set to $0.25Hz/s$ and the damping ratio is assumed to be 0.001. The blade 1 responses at the two resonances are plotted in Fig. 8 (grey curves). The simulated sensors signals are shown on the same figures. The sensor signals are then fitted (by the transient fit model) by using only the data after the maximum amplitude toward the beating vibrations.

The results of the fitting in the form of response envelope are shown in Fig. 9. The results are normalized with respect to the peak amplitude. It can be seen that the transient SDOF model successfully fits the exact response curve. On the contrary the result of the fitting by a steady state model (green curve) does not match with the exact response curve. Table 2 reported the estimated parameters obtained by the fitting with the standard steady state model and the transient model. As observed, very good predictions of the parameters are achieved by the transient model. On the other hand, the steady state model gives good prediction of the natural frequencies but the estimate of the damping ratio is completely wrong (errors from 50% to 134%). Even the estimate of the amplitude at resonance by the steady state model is not so good (error from 6% to 8%).
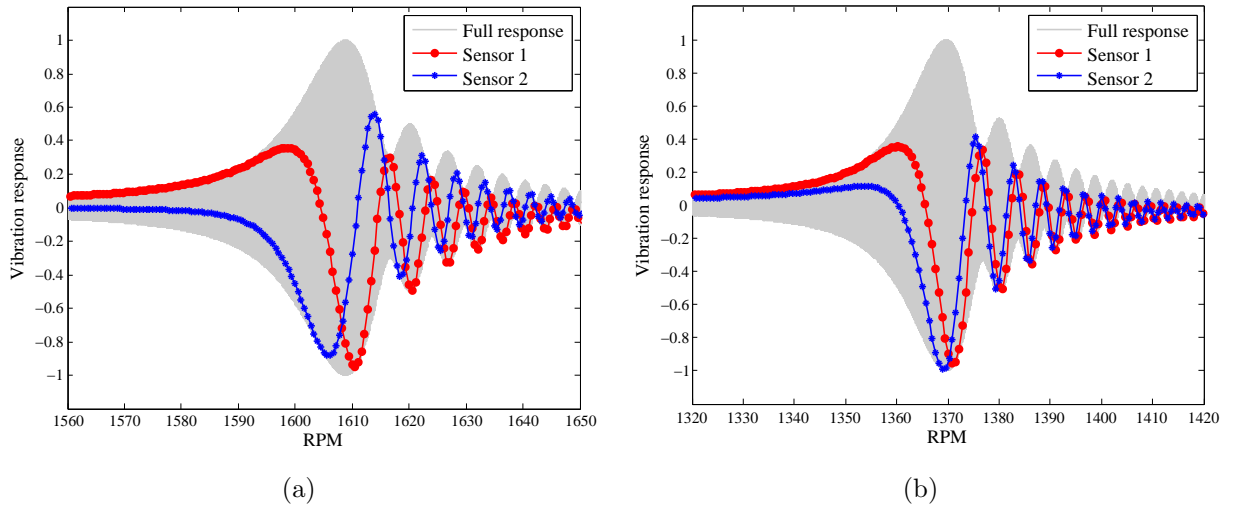

(a)   (b)

Figure 8: Vibration response and the BTT data for two different resonance cases at the rotating speed sweep rate of $0.25Hz/s$ and $\zeta = 0.001$, (a) EO=6 , ND=6 , (b) EO=7 , ND=5.

The sweep rate of the excitation frequency is a key factor that strongly influences the dynamic response. In fact, the transient effects will be magnified by increasing the sweep rate. For this reason, the capability of the transient fitting model is further examined for
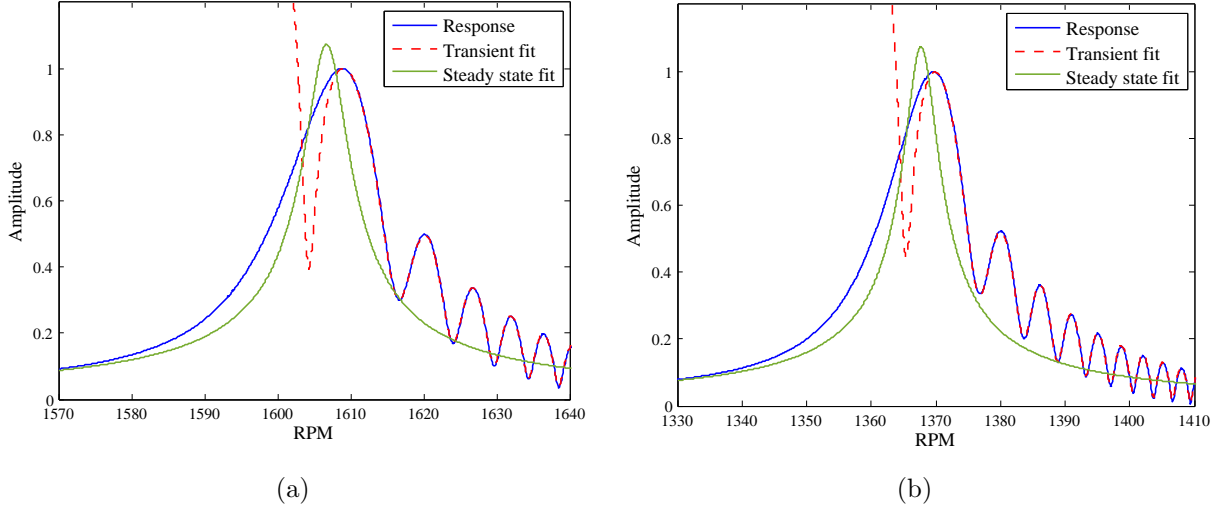
16

Figure 9: Amplitude obtained by the steady state and transient models for two different resonance cases at the rotating speed sweep rate of $0.25Hz/s$ and $\zeta = 0.001$, (a) EO=6 , ND=6 , (b) EO=7 , ND=5.

signals obtained under different sweep rates. Fig. 10 shows the results of the fitting for the two low and high rotating speed sweep rates with the values of $0.125Hz/s$ and $0.50Hz/s$, respectively. Here, the EO=6 excites the ND=6. From figure 10, it can be observed that even at these different speed sweep rates, the response obtained by the transient fitting model is well overlapped with the exact response curve.

The results of the transient fitting models are presented in Table 3 together with the parameters obtained by the steady state fitting model.

The transient model confirms to be much more accurate than the steady state model in the prediction of the parameters, especially in the prediction of the damping ratio. The errors of the estimated parameter from the transient model are all below 1%, while the steady state model gives unacceptable errors (greater than 80%) on the estimate of the damping ratio. Fig. 11 displays the effect of different sweep rates on the identified value of the damping ratio. It can be observed that the transient model leads to significantly lower errors.

3.2.2. Damping effect

The transient response (with the associated beating phenomenon) is typical of a system with very low damping. This could be the case of blisks (integrally bladed disks) or of bladed disks in laboratory conditions in absence of aerodynamic damping. Both the decreasing of the damping or the increasing of sweep rate give a response across the resonance with a
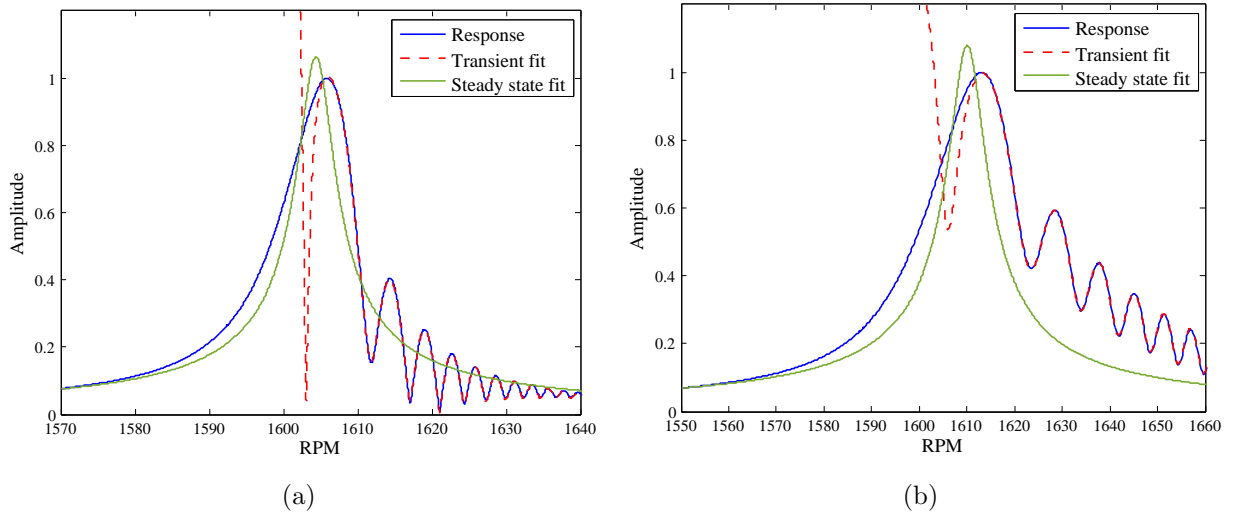
17

Figure 10: Amplitude obtained by the steady state and transient models for two rotating speed sweep rates and $\zeta = 0.001$ at EO=6, ND=6 and, (a) 0.125 Hz/s, (b) 0.50 Hz/s.
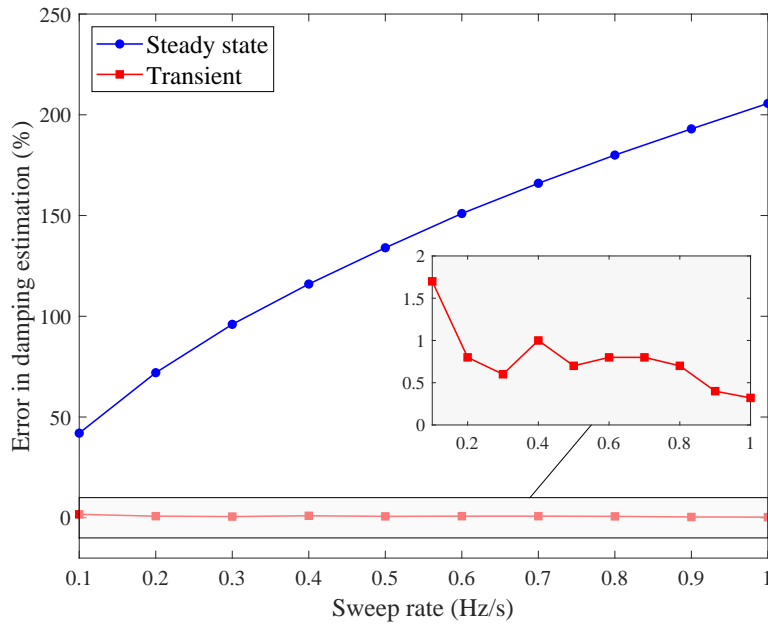

Figure 11: Sweep rate effect on the identification of damping ratio for $\zeta = 0.001$ at EO=6, ND=6.

strong transient behavior.

The fitting procedure using the transient model or the steady state model was then applied to the same system with different damping values at the same sweep rate. The errors of the estimated damping values (by both models) are plotted in Fig. 12. This graph

Table 2: Comparison of the vibration parameters identified by the steady state and transient models for two different resonance cases at the rotating speed sweep rate of $0.25 Hz/s$.

Parameter	Exact value	Steady State Model	Difference (%)	Transient Model	Difference (%)
			EO=6 , ND=6		
Frequency (Hz)	160.02	160.67	0.41	160.02	0.00
Damping ratio	1.00e-3	1.84e-3	84.42	9.92e-4	0.75
Max. amplitude	1.00	1.07	7.43	99.95e-2	0.05
			EO=7 , ND=5		
Frequency (Hz)	158.86	159.57	0.45	158.86	0.00
Damping ratio	1.00e-3	1.93e-3	93.22	9.90e-4	1.00
Max. amplitude	1.00	1.07	7.40	99.84e-2	0.16

Table 3: Comparison of the vibration parameters identified by the steady state and transient models for two rotating speed sweep rates at EO=6 and ND=6

Parameter	Exact value	Steady State Model	Difference (%)	Transient Model	Difference (%)
			0.125 Hz/sec		
Frequency (Hz)	160.02	160.44	0.26	160.02	0.00
Damping ratio	1.00e-3	1.50e-3	50.15	9.88e-4	1.21
Max. amplitude	1.00	1.06	6.45	1.01	0.70
			0.50 Hz/sec		
Frequency (Hz)	160.02	161.01	0.61	160.02	0.00
Damping ratio	1.00e-3	2.34e-3	134.37	9.93e-4	0.71
Max. amplitude	1.00	1.08	8.02	9.98e-1	0.17

gives an overall perspective of the fitting models performance.

It is clear from the figure that for the low damping values, the errors of the transient model are much less than the steady state model. This can be attributed to the fact that by decreasing damping, the transient effect becomes pronounced in the vibrating response and the transient model works greatly better than the steady state model, while for the high values of the damping ratio due to diminishing of the transient effect, the steady state model works relatively better.

An example of a response with high damping ratio ($\zeta = 0.01$), is shown in Fig. 13. It can be seen that the curve from the fitting using the steady state model is completely overlapped, on the entire resonance region, with the exact response curve. On the other hand, the curve fitted by the transient model could cover only half of the resonance region. The error in damping estimation in the case of the steady state model is low (around 1%) but still acceptable (around 4%) in the case of the transient model. The drawback is that in this case with high damping the transient model is not able to capture the peak amplitude value.
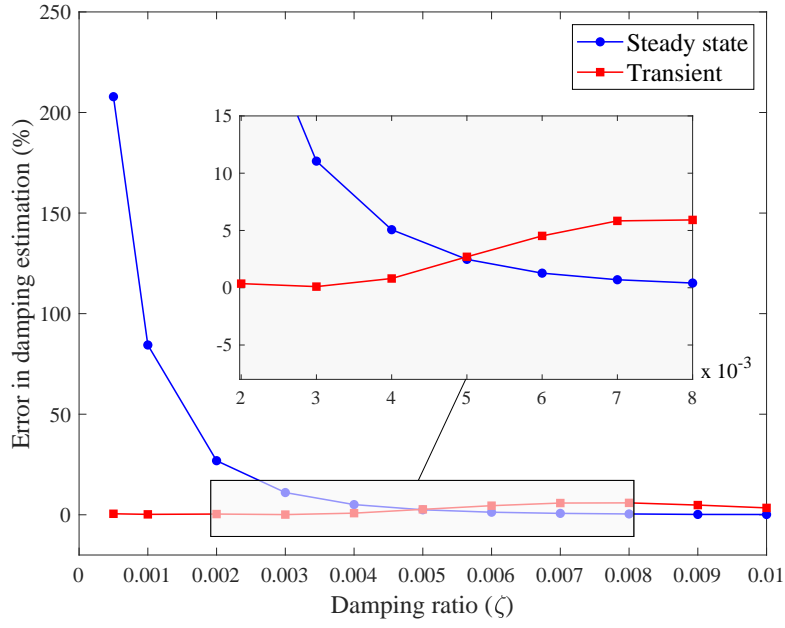
Figure 12: Errors in the damping estimation by the steady state and transient models for the rotating speed sweep rate of $0.25Hz/s$ at EO=6, ND=6.
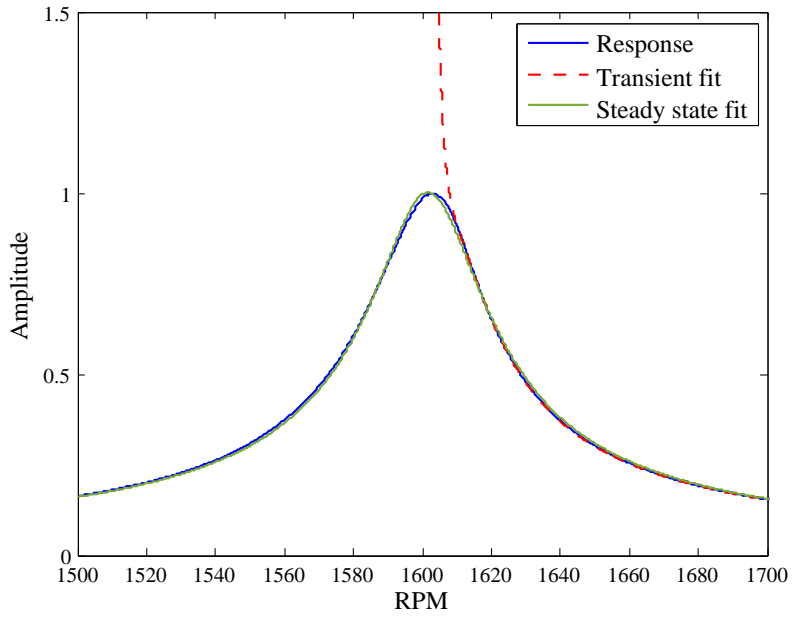

Figure 13: Amplitude obtained by the steady state and transient models for the rotating speed sweep rates of $0.25Hz/s$ with $\zeta = 0.01$ at EO=6, ND=6.
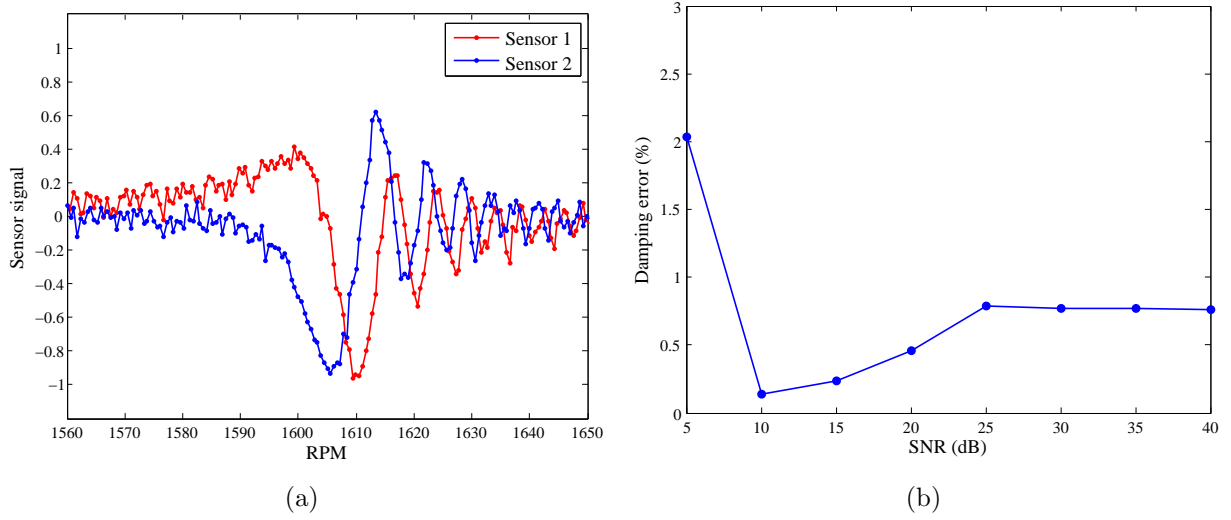
Figure 14: Sensor data contaminated by noise for the resonances at EO=6 and ND=6, (a) Typical noisy signals SNR=5 dB, (b) Errors in damping ratio.

3.2.3. Noise effect

During the vibration measurement, the signals recorded by the sensors are generally contaminated by the noise originating from different sources. Although the noise is usually reduced by the filtering algorithms, some noise can still be present in the acquired sensor signals. A white Gaussian noise is then added to the BTT signals numerically generated for the resonances excited by EO=6 in ND=6. Different intensities of the noise is added to the original signal by adjusting the values of the Signal to Noise Ratio (SNR). The typical sensors signals contaminated by noise are shown in Fig. 14 (a). Fig. 14 (b) shows the percentage errors in the estimation of the damping ratio for different SNR in the sensors signals. The error in the damping ratio estimation increases by increasing the noise level (decreasing SNR), but the error keeps below 2%, which can be considered still an acceptable error value.

4. Experimental validation

In order to verify its capability to extract the vibration parameters, the transient SDOF fitting model was applied to experimental data. The experimental data were obtained by BTT and strain gauges on a laboratory spinning rig with a rotating bladed disk as described in the next sections.

21

Figure 15: The experimental test case.

4.1. Experimental test case

The test case (Fig. 15) is a bladed disk with 12 blades which is integrally machined from a single piece of an aluminum 5 mm thick flat plate. The blades are cantilever beams with a rectangular geometry having a length of 150 mm and a width of 25 mm, the tip radius is 200 mm.

A numerical computation by a finite element code provided the natural frequencies and the corresponding mode shapes of the disk. The computation is performed by a cyclic symmetry modal analysis. The Campbell diagram obtained for the first modal family in a range of rotational speed up to 3000 RPM is depicted in Fig. 16. The first modal family corresponds to the first bending mode vibrating out of plane. In the same figure the EO excitation lines cross the first modal family lines at the critical speeds at which the resonances can be excited.

Before the tip timing measurements, in order to identify the dynamics main parameters of the test case, an experimental modal analysis was performed by impact testing. The impact tests were carried out in the spinning rig, but with the disk not rotating, in order to have the same shaft-disk constrain conditions as during the rotating tests. A scanning laser vibrometer was used to measure the response of the disk in terms of deformed operative shape. An example of the obtained FRFs, the FRF of blade 1, is shown in Fig. 17. In the figure the resonances peaks are labeled with the corresponding nodal diameters.
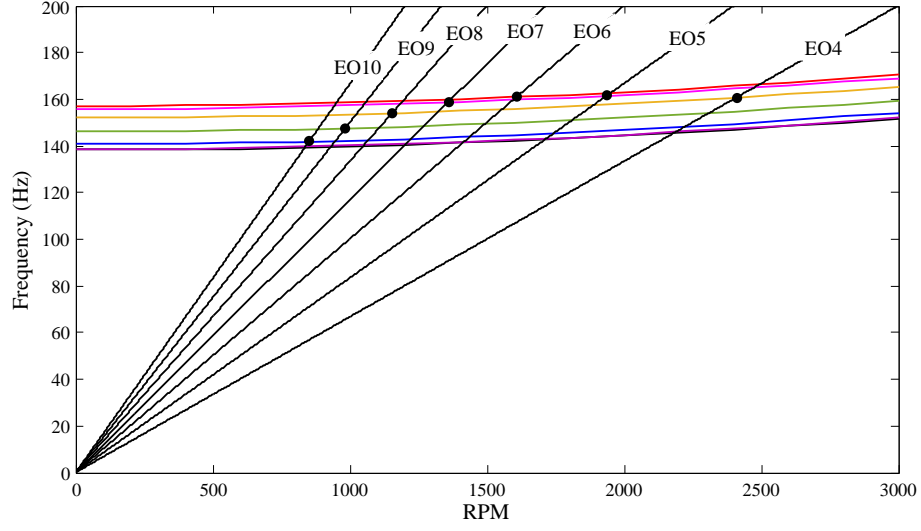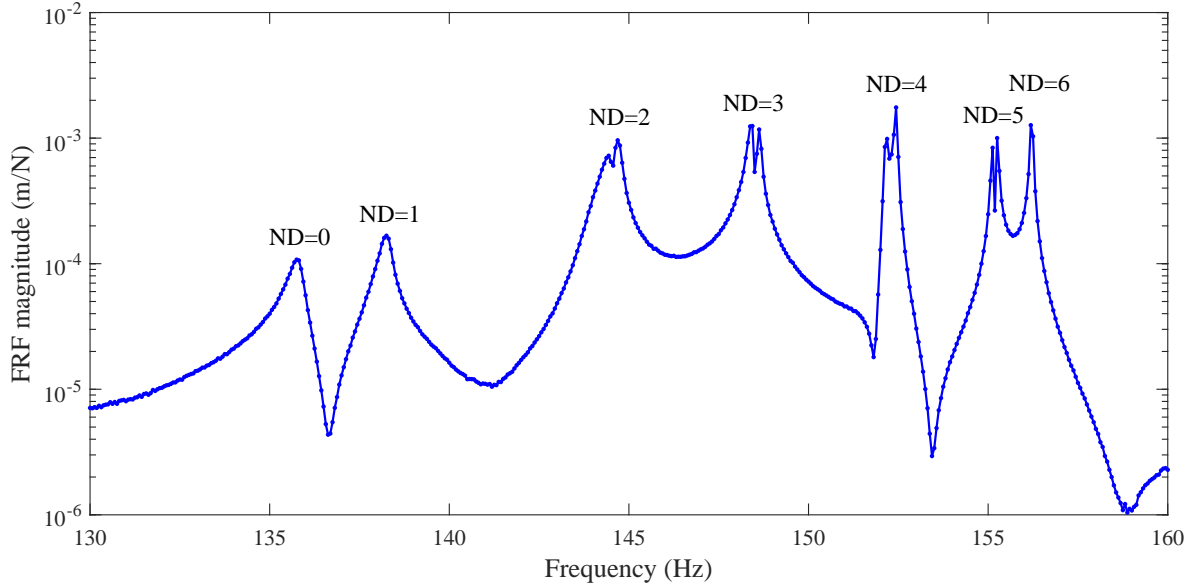
Figure 16: Campbell diagram of the test case.

Figure 17: FRF obtained by hammer test for blade 1.

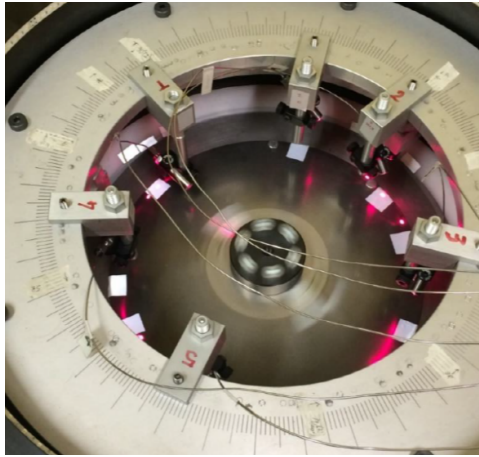## 4.2. Experimental setup (BTT and strain gauge)

In Fig. 18(a) the bladed disk rotating within the test rig chamber is instrumented by the BTT sensors. The rotating tests are carried out in vacuum conditions. Five fiber optical sensors located at the angular positions of 90°, 203°, 244°, 281° and 310° were employed to measure the tip timing signals. The BTT is a commercial system developed by the Hood

23

Technology Corporation [37]. The system employs optical shutter sensors where each sensor is split into an optical "sender" and an optical "receiver". Sensors generate analog pulses each time a blade passes in front of them. A remotely-powered preamplifier is connected to the sensors. The preamplifier receives power and sends buffered signals to the Blade Vibration Sensor Interface (BVSI) unit. The acquisition system has 30 channels, with a clock speed of 80MHz. The signals are processed in real time by a software application in the LabView environment.

Since the first modal family of the blades is associated with the out of plane bending mode; the blade tip deflection can not be detected by placing the probes in the radial direction as shown in the scheme of Fig. 2. It was therefore necessary to design a new sensor configuration. In this configuration as depicted in Fig. 18(b), the sensors are positioned along the rotational axis facing toward the bladed disk and then tilted 45° along the circumferential direction. Each sensor works as a sender and a receiver thanks to a reflective tape positioned on the stationary part below the disk. An extra sensor (OPR sensor) provides the timing reference and the rotating speed measurement.

The excitation forces are generated by a permanent magnet facing the disk. The magnet is connected to a static flange at a fixed distance from the bladed disk. Moreover, a permanent magnet is inserted into the tip of each blade, this guarantees the excitation of the blades while passing in front of the external fixed magnet.
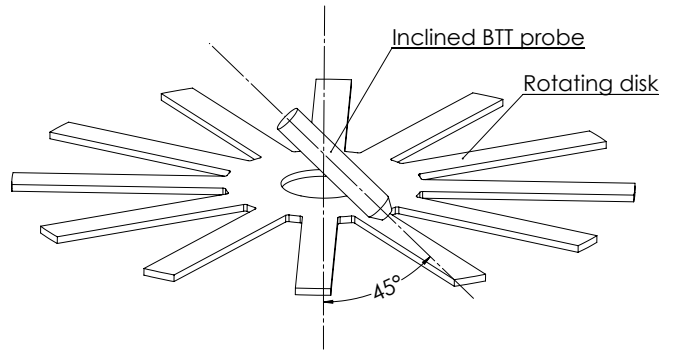
| (a) | (b) |

Figure 18: The BTT experimental setup (a) and the sensors positioning (b).

In order to validate the BTT measurements, strain gauge measurements are performed at the same time as BTT. Two blades (blade 1 and blade 7) have been selected to be equipped

24

with strain gauges. On each blade the strain gauge was glued at the root near the blade and disk attachment area (see Fig. 15) since this is a region of high strain for the considered mode shape. The sampling frequency of the strain gauges is 8192 Hz and the measured signals are transmitted through a telemetry system to the external data acquisition system. The same transient SDOF model used to fit the BTT sensors signals was used to fit the strain gauge signals. In the case of the strain gauges, the transient SDOF model is applied to the amplitude of the measured strain. The vibration parameters are then determined by fitting the measured strain amplitude by the same SDOF model used for fitting (magnitude of Q in Eq. 13). The parameters obtained from the fitting of the strain gauges data can be considered as reference values since the strain gauges signals are better sampled (higher sampling frequency) than the BTT signals.

4.3. Test results

The experiments were focused on the excitation of ND=5 and ND=6 with EO=7 and EO=6, respectively. To do this, the shaft speed was ramped up from 600 RPM to 2600 RPM during a time interval of 2140 s with a linear sweep rate of 0.0156 Hz/s.

ND=5 and ND=6 were selected since they correspond to two cases of well isolated peaks. As shown in Fig. 17 in fact, in ND=5 the peaks are very well separated while in correspondence of ND=6 there is only one dominant peak.

The data recorded by the strain gauge and the BTT sensors over the speed sweep are shown in Fig. 19 for the blade 1 when EO=6 excites ND=6. All the BTT sensor signals are given as vibration response (displacement), since the software converts the time of arrival in displacement by Eq. 3. In this conversion the speed is assumed constant over a single revolution. Including the speed change already in this computation step would have led to a variation in the displacement less than 0.004% which can be considered negligible.

Both the steady state and transient SDOF models were tested on the data measured by the strain gauges and the BTT probes. The results of fitting are reported in Fig. 20. For the strain gauge, as already explained in subsection 4.2, the amplitude of the measured strain (strain envelope) is extracted at first, shown by blue curve in Fig. 20(a) and then the fitting algorithm is applied on it. Finally, based on the resonance parameters obtained by the fitting procedure, the fitted amplitude is reconstructed. For the BTT, as stated earlier in the subsection 2.3, the fitting is performed on all sensors data together as shown in Fig. 5. However, for better comparison and for the sake of consistency with strain gauge results, the response envelope constructed by the traditional Sine fitting algorithm [22] is depicted in the BTT figures instead of showing the fitted curves for each sensor. Sine fitting employs
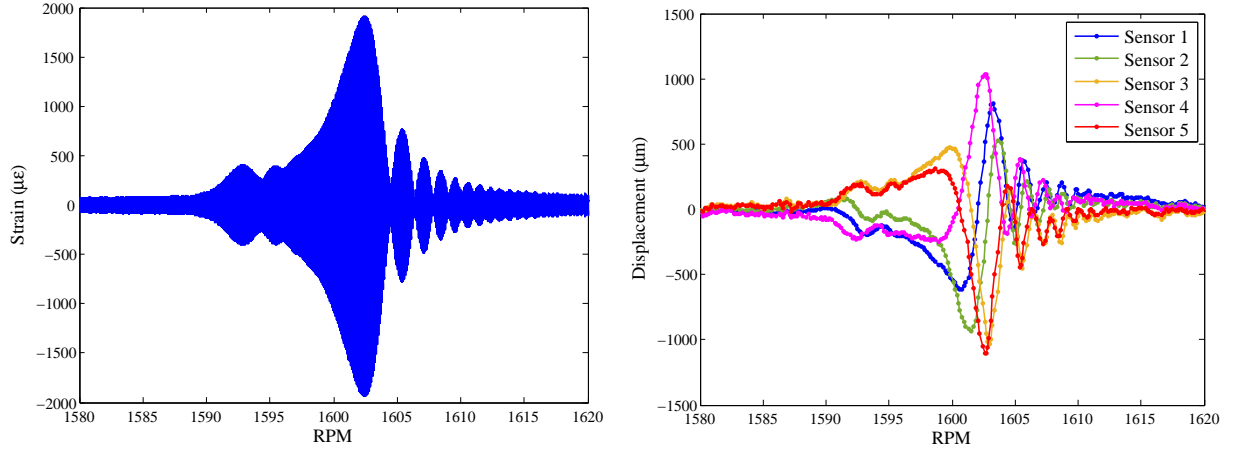
Figure 19: Strain and BTT displacement measurements for blade 1 corresponding to EO=6 and ND=6.
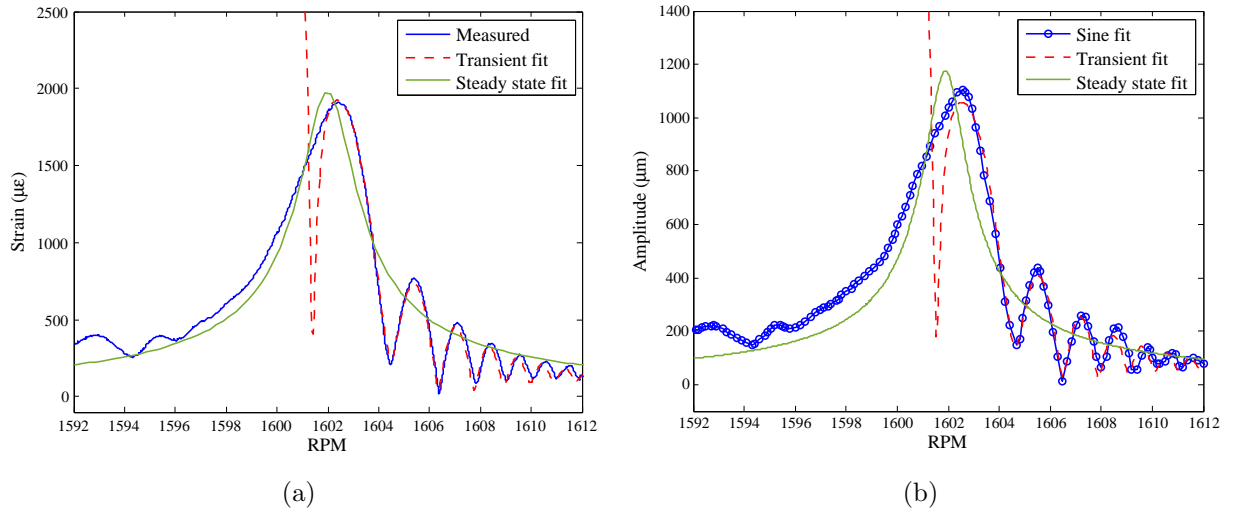

Figure 20: Fitting results for blade 1 corresponding to EO=6 and ND=6, (a) strain gauge, (b) BTT.

a sinusoidal wave with a constant amplitude and frequency to the data acquired by the sensors in each revolution. By sweeping the rotating speed and employing this method, the amplitude curve can be reconstructed in the resonance region.

It can be observed that a very good fitting is achieved by the transient SDOF model for both the strain gauges and the BTT measurements, it can in fact be observed that the fitted curves successfully capture the beating phenomenon. For blade 7, the fitting results are plotted in Fig. 21. Even in this case, the transient SDOF model provides accurate fitting for both BTT and strain gauges data.

The vibration parameters computed by the fitting analysis both on strain gauge and BTT
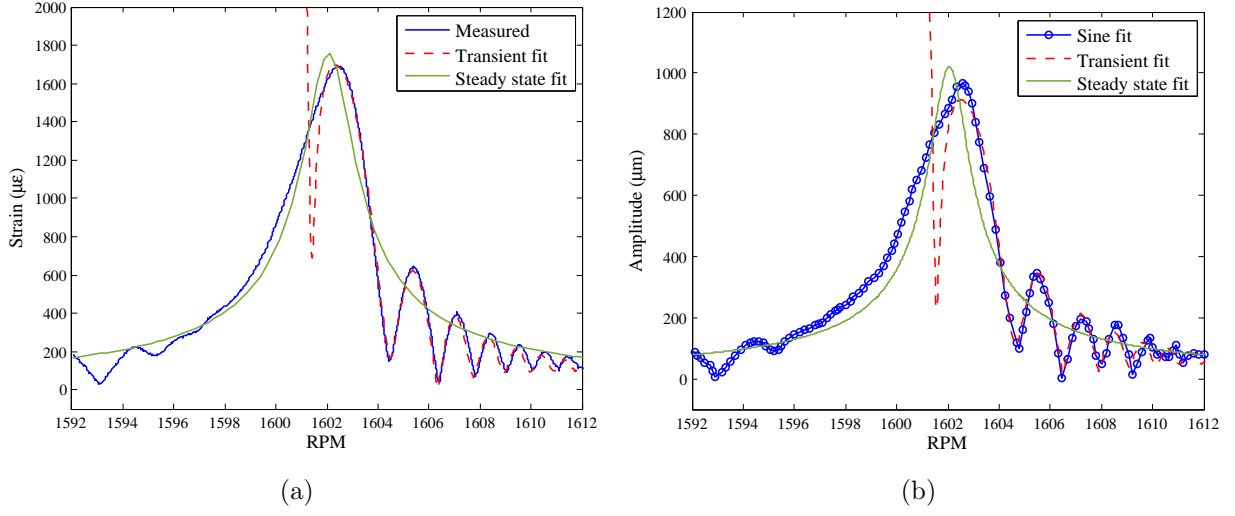
26

Figure 21: Fitting results for blade 7 corresponding to EO=6 and ND=6, (a) strain gauge, (b) BTT.

signals are reported in Table 4. It can be seen that the difference in the values obtained for the resonance frequency by strain gauge and BTT is very small (less than 1%) when using the transient fit method for both. This small difference is confirmed if the steady state fit method is used instead of the transient fit. Using the steady state fit method therefore seems acceptable to obtain the value of the resonant frequency. The main differences are instead observed in the estimation of the damping ratio. In fact, if the transient fit method is used, the difference between the value obtained with the strain gauge and that obtained with the BTT is less than 4.5 %. On the contrary, if the steady state fit method is used, the difference between the value obtained with the strain gauge and that obtained with the BTT is greater than 20 %. Most importantly, the damping values estimated by the steady state model are much higher than those of the transient model. Moreover by looking at Fig. 20 and Fig. 21 it can be observed that the steady state fit (green curve) for both strain gauge and BTT overpredict the amplitude of the response at the resonance frequency. These results confirm the results obtained on the numerical test case reported in Table 2 and Table 3. In that case the "exact" values of the damping ratio, frequency and amplitude at resonance were known beforehand. The steady sate fit method proved to be very inaccurate to obtain the values of the damping ratio (errors up to 135%) and of the amplitude at resonance (errors up to 8%). It must be also noted that these estimation errors increased as the speed sweep rate increases.

In the second step of the experimental validation, the resonance peak corresponding to ND=5 (excited by EO=7) around the rotating speed of 1350 RPM is considered. The

Table 4: Comparison of the identified vibration parameters for EO=6 and ND=6.

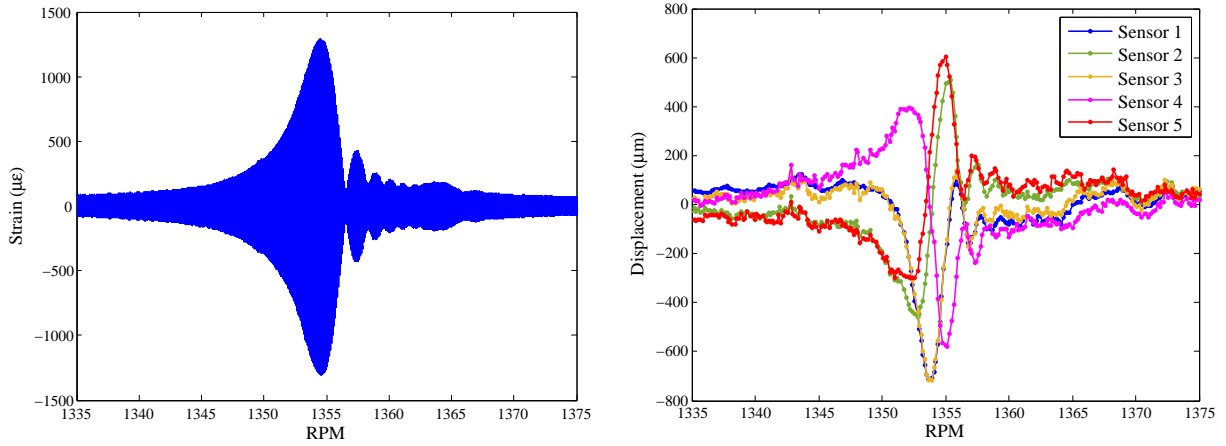|	Steady state model			Transient model		
	Strain gauge	BTT	Difference (%)	Strain gauge	BTT	Difference (%)
Parameters			Blade 1			
Frequency (Hz)	160.20	160.19	0.01	160.04	160.05	0.01
Damping ratio	6.54e-04	5.12e-04	21.71	3.71e-04	3.67e-04	1.08
			Blade 7			
Frequency (Hz)	160.21	160.21	0.00	160.04	160.06	0.01
Damping ratio	6.02e-04	4.79e-04	20.43	3.94e-04	3.77e-04	4.31

Figure 22: Strain and BTT displacement measurements for blade 1 corresponding to EO=7 and ND=5.

signals measured by strain gauge and BTT on the blade 1 are shown in Fig. 22. The fitted curves of strain gauge and BTT for blade 1 and blade 7 are reported in Fig. 23 and Fig. 24. The parameters obtained for the two blades by the fitting are listed in Table 5. The same comments of the results obtained for ND=6 hold for this case of ND=5. The difference between the parameters estimated with strain gauge and BTT, in particular for the damping ratio, is much smaller in the case of using the transient fit model rather than the steady state fit. This is a further proof that using the transient fit model for data fitting leads to more accurate results. Additionally, the transient effect and the associated beating phenomenon are not much significant in the current resonance compared to the EO=6 and ND=6 and therefore, the damping values estimated by the transient model are closer to the values predicted by the steady state model.

5. Concluding remarks

In this paper we proposed a transient model to fit the BTT or strain gauge measured data in those cases where the blade response deviates from the steady state behavior and
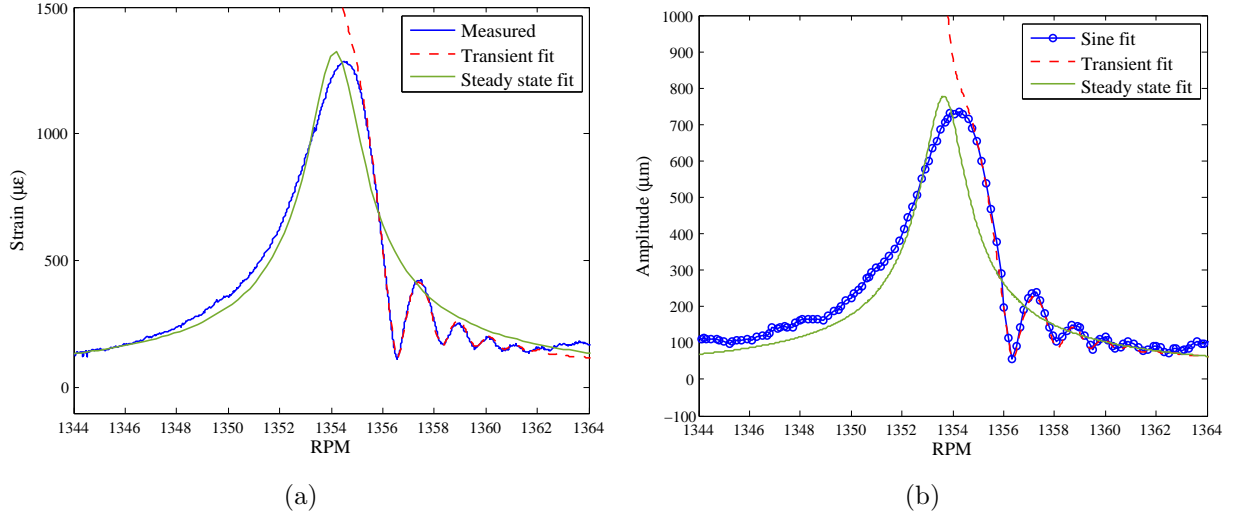
Figure 23: Fitting results for blade 1 corresponding to EO=7 and ND=5, (a) strain gauge, (b) BTT.

Table 5: Comparison of the identified vibration parameters for EO=7 and ND=5.

	Steady state model			Transient model		
	Strain gauge	BTT	Difference (%)	Strain gauge	BTT	Difference (%)
Parameters	Blade 1					
Frequency (Hz)	157.99	157.92	0.04	157.82	157.80	0.01
Damping ratio	7.58e-04	6.31e-04	16.75	6.30e-04	6.15e-04	2.22
	Blade 7					
Frequency (Hz)	157.99	157.94	0.03	157.82	157.80	0.01
Damping ratio	7.40e-04	6.36e-04	14.05	7.02e-04	6.89e-04	1.90

presents a "beating" phenomenon.

The proposed method was firstly validated on a numerical test case, a lumped parameters model of a bladed disk, where the "true" vibration parameters were already known. The simulated data were fitted using both the classical steady state model and the proposed transient fit model, obtaining the main vibrations parameter to compare with the "true" values. From this numerical validation it was observed that:

– the fitting transient model provided very accurate estimates of all the parameters with errors always lower than 2% for the different values of the speed sweep rate, even in presence of a simulated noise of a standard level;

– on the contrary, the steady state fit model was enough accurate only for the estimate of the resonance frequency, while it led to huge errors (even higher than 100%) in the estimation of the damping ratio and it overestimates (up to 8%) the amplitude at resonance;
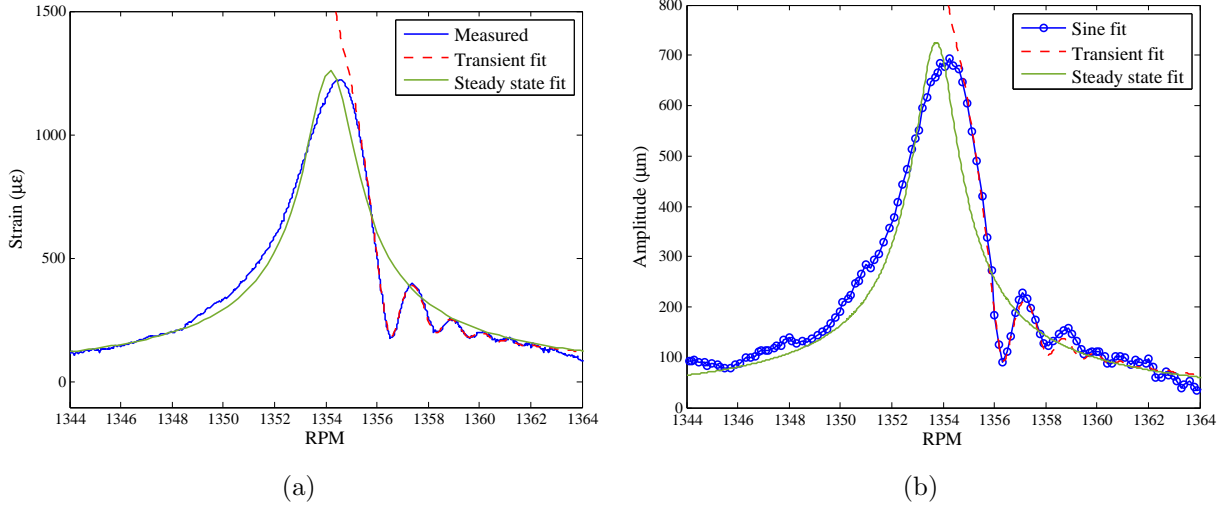
29

Figure 24: Fitting results for blade 7 corresponding to EO=7 and ND=5, (a) strain gauge, (b) BTT.

   − these estimation errors of the steady state fit model increase when the response signals were sampled in a condition further and further away from the stationary condition, i.e. as the speed sweep rate increases (from 0.125 Hz/s to 0.50 Hz/s).

In a second validation step, the proposed method was applied to experimental data. In this case, unlike the numerical case, the true values of the parameters were not known in advance but it was possible to compare the values of the parameters obtained by the two measurement systems (strain gauge and BTT). It was confirmed that the proposed transient model works better than the classical steady state model in presence of beating. Especially in the estimation of the damping where the classical steady state model overpredicts the damping ratio, giving a value more than 20% higher.

It was then proved that, in presence of beating in the response, the use of the transient model is preferable, especially if accuracy on the damping ratio is requested. One of the drawbacks of the identification procedure, using the transient model, is the nonlinear fitting of the sensors data. As a consequence, the transient method works well with suitable initial guesses of the model parameters. It can then be suggested that the two methods (steady state and transient) are used in series since the steady state model usually converges more rapidly than the transient method. If the steady state model does not satisfactory fit the data, the results of its fitting can be used as starting points of the nonlinear fitting of the transient model.

References

[1] M. A. Gonzalez-Salazar, T. Kirsten, L. Prchlik, Review of the operational flexibility and emissions of gas-and coal-fired power plants in a future with growing renewables, Renewable and Sustainable Energy Reviews 82 (2018) 1497–1513.

[2] M. Nimtz, H.-J. Krautz, Flexible operation of ccs power plants to match variable renewable energies, Energy Procedia 40 (2013) 294–303.

[3] D. J. Ewins, Modal testing: theory, practice and application, John Wiley & Sons, 2009.

[4] J. P. Ayers, D. M. Feiner, J. H. Griffin, A Reduced-Order Model for Transient Analysis of Bladed Disk Forced Response, Journal of Turbomachinery 128 (3) (2005) 466–473.

[5] F. M. Lewis, Vibration during acceleration through a critical speed, Trans. Am. Soc. Mech. Eng. 54 (1932) 253.

[6] R. Fearn, K. Millsaps, Constant acceleration of an undamped simple vibrator through resonance, The Aeronautical Journal 71 (680) (1967) 567–569.

[7] R. Markert, M. Seidler, Analytically based estimation of the maximum amplitude during passage through resonance, International Journal of Solids and Structures 38 (10-13) (2001) 1975–1992.

[8] C. C. Reed, A. M. Kobe, Peak response of single degree of freedom systems to swept frequency excitation, The Mathematica Journal 21.

[9] J. Slater, G. Minkiewicz, A. Blair, Forced response of bladed disk assemblies-a survey, in: 34th AIAA/ASME/SAE/ASEE Joint Propulsion Conference and Exhibit, 1999, p. 3743.

[10] M. P. Castanier, C. Pierre, Modeling and analysis of mistuned bladed disk vibration: current status and emerging directions, Journal of Propulsion and power 22 (2) (2006) 384–396.

[11] A. Hartung, A numerical approach for the resonance passage computation, in: Turbo Expo: Power for Land, Sea, and Air, Vol. 44014, 2010, pp. 723–728.

[12] M. Bonhage, L. Panning-von Scheidt, J. Wallaschek, C. Richter, Transient resonance passage with respect to friction, in: Turbo Expo: Power for Land, Sea, and Air, Vol. 44731, American Society of Mechanical Engineers, 2012, pp. 1227–1237.

[13] M. Bonhage, O. P. Hentschel, L. Panning-v. Scheidt, J. Wallaschek, Transient amplification of maximum vibration amplitudes, PAMM 15 (1) (2015) 47–48.

[14] M. Bonhage, J. T. Adler, C. Kolhoff, O. Hentschel, K.-D. Schlesier, L. Panning-von Scheidt, J. Wallaschek, Transient amplitude amplification of mistuned structures: An experimental validation, Journal of Sound and Vibration 436 (2018) 236–252.

[15] Y. Kaneko, Study on transient vibration of mistuned bladed disk passing through resonance, in: Turbo Expo: Power for Land, Sea, and Air, Vol. 55270, American Society of Mechanical Engineers, 2013, p. V07BT31A002.

[16] B. Lübbe, C. Siewert, Optimization of the vibration behavior at speed-synchronous resonance of a large turbine blade during speed-up and coast-down under consideration of mistuning, in: Turbo Expo: Power for Land, Sea, and Air, Vol. 50954, American Society of Mechanical Engineers, 2017, p. V008T29A013.

[17] L. Carassale, M. Marrè-Brunenghi, S. Patrone, Estimation of damping for turbine blades in non-stationary working conditions, in: Turbo Expo: Power for Land, Sea, and Air, Vol. 56772, American Society of Mechanical Engineers, 2015, p. V07BT32A018.

[18] L. Carassale, M. Marrè-Brunenghi, S. Patrone, Modal identification of dynamically coupled bladed

disks in run-up tests, in: Turbo Expo: Power for Land, Sea, and Air, Vol. 49835, American Society of Mechanical Engineers, 2016, p. V07AT32A018.

[19] L. Carassale, M. Marrè-Brunenghi, S. Patrone, Wavelet-based identification of rotor blades in passage-through-resonance tests, Mechanical Systems and Signal Processing 98 (2018) 124–138.

[20] I. Y. Zablotskiy, Y. A. Korostelev, Measurement of resonance vibrations of turbine blades with the elura device, Tech. rep., Foreign Technology Div Wright-Patterson AFB OH (1978).

[21] S. Heath, A new technique for identifying synchronous resonances using tip-timing, Journal of Engineering for Gas Turbines and Power 122 (2) (2000) 219–225.

[22] S. Heath, A study of tip-timing measurement techniques for the determination of bladed-disk vibration characteristics.

[23] I. B. Carrington, J. R. Wright, J. Cooper, G. Dimitriadis, A comparison of blade tip timing data analysis methods, Proceedings of the Institution of Mechanical Engineers, Part G: Journal of Aerospace Engineering 215 (2001) 301 – 312.

[24] D. Heller, I. Sever, C. Schwingshackl, A method for multi-harmonic vibration analysis of turbomachinery blades using blade tip-timing and clearance sensor waveforms and optimization techniques, Mechanical Systems and Signal Processing 142 (2020) 106741.

[25] S. Heath, M. Imregun, An improved single-parameter tip-timing method for turbomachinery blade vibration measurements using optical laser probes, International Journal of Mechanical Sciences 38 (10) (1996) 1047 – 1058.

[26] G. Schlagwein, U. Schaber, Non-contact blade vibration measurement analysis using a multi-degree-of-freedom model, Proceedings of the Institution of Mechanical Engineers, Part A: Journal of Power and Energy 220 (6) (2006) 611–618.

[27] P. Russhard, Development of a blade tip timing based engine health monitoring system, The University of Manchester, 2010.

[28] H. Guo, F. Duan, J. Zhang, Blade resonance parameter identification based on tip-timing method without the once-per revolution sensor, Mechanical Systems and Signal Processing 66-67 (2016) 625 – 639.

[29] G. Rigosi, G. Battiato, T. M. Berruti, Synchronous vibration parameters identification by tip timing measurements, Mechanics Research Communications 79 (2017) 7 – 14.

[30] G. Battiato, C. Firrone, T. Berruti, Forced response of rotating bladed disks: Blade tip-timing measurements, Mechanical Systems and Signal Processing 85 (2017) 912–926.

[31] S. Bornassi, M. Ghalandari, S. F. Maghrebi, Blade synchronous vibration measurements of a new upgraded heavy duty gas turbine mgt-70 (3) by using tip-timing method, Mechanics Research Communications 104 (2020) 103484.

[32] S. Bornassi, C. M. Firrone, T. M. Berruti, Vibration parameters estimation by blade tip-timing in mistuned bladed disks in presence of close resonances, Applied Sciences 10 (17) (2020) 5930.

[33] S. Wu, Z. Zhao, Z. Yang, S. Tian, L. Yang, X. Chen, Physical constraints fused equiangular tight frame method for blade tip timing sensor arrangement, Measurement 145 (2019) 841–851.

[34] S. S. Rao, Vibration of continuous systems, Vol. 464, Wiley Online Library, 2007.

[35] S.-Y. Lee, M. Castanier, C. Pierre, Assessment of probabilistic methods for mistuned bladed disk vibration, in: 46th AIAA/ASME/ASCE/AHS/ASC Structures, Structural Dynamics and Materials

Conference, 2005, p. 1990.

[36] T. Zhao, H. Yuan, W. Yang, H. Sun, Genetic particle swarm parallel algorithm analysis of optimization arrangement on mistuned blades, Engineering Optimization 49 (12) (2017) 2095–2116.

[37] Hood Technology, Overview of Blade Vibration Monitoring Capabilities, Hood Technology Corporation, June 2011.